

Skeletal calcification patterns of batoid, teleost, and mammalian models: Calcified cartilage versus bone matrix

Ugo E. Pazzaglia^{1,2}  | Marcella Reguzzoni²  | Chiara Milanese³  |
Renata Manconi⁴  | Luca Lanteri⁵  | Tiziana Cubeddu⁴  | Guido Zarattini¹  |
Piero A. Zecca²  | Mario Raspanti² 

¹DSMC, University of Brescia, Brescia, Italy

²DMC, University of Insubria, Varese, Italy

³CSGI, Physical Chemistry Division, University of Pavia, Pavia, Italy

⁴DVM, University of Sassari, Sassari, Italy

⁵DISTAV, University of Genova, Genoa, Italy

Correspondence

Ugo E. Pazzaglia, DSMC, University of Brescia, Brescia, Italy.

Email: u.e.pazzaglia@gmail.com

Marcella Reguzzoni, DMC, University of Insubria, Varese, Italy.

Click here to enter text.

Email: marcella.reguzzoni@uninsubria.it

Review Editor: Alberto Diaspro

Abstract

This study compares the skeletal calcification pattern of batoid *Raja asterias* with the endochondral ossification model of mammals *Homo sapiens* and teleost *Xiphias gladius*. Skeletal mineralization serves to stiffen the mobile elements for locomotion. Histology, histochemistry, heat deproteination, scanning electron microscopy (SEM)/EDAX analysis, thermogravimetric analysis (TGA), differential scanning calorimetry (DSC), and Fourier transform infrared spectrometry (FTIR) have been applied in the study. *H. sapiens* and *X. gladius* bone specimens showed similar profiles, *R. asterias* calcified cartilage diverges for higher water release and more amorphous bioapatite. In endochondral ossification, fetal calcified cartilage is progressively replaced by bone matrix, while *R. asterias* calcified cartilage remains un-remodeled throughout the life span. Ca^{2+} and PO_4^{3-} concentration in extracellular matrix is suggested to reach the critical salts precipitation point through H_2O recall from extracellular matrix into both chondroblasts or osteoblasts. Cartilage organic phase layout and incomplete mineralization allow interstitial fluids diffusion, chondrocytes survival, and growth in a calcified tissue lacking of a vascular and canalicular system.

Highlights

- Comparative physico-chemical characterization (TGA, DTG and DSC) testifies the mass loss due to water release, collagen and carbonate decomposition of the three tested matrices.
- *R. asterias* calcified cartilage water content is higher than that of *H. sapiens* and *X. gladius*, as shown by the respectively highest dehydration enthalpy values.
- Lower crystallinity degree of *R. asterias* calcified cartilage can be related to the higher amount of collagen in amorphous form than in bone matrix.
- These data can be discussed in terms of the mechanostat theory (Frost, 1966) or by organic/inorganic phase transformation in the course evolution from fin to limbs.
- Mineral analysis documented different characters of *R. asterias* vs *H. sapiens* and *X. gladius* calcified matrix.

This is an open access article under the terms of the [Creative Commons Attribution](https://creativecommons.org/licenses/by/4.0/) License, which permits use, distribution and reproduction in any medium, provided the original work is properly cited.

© 2023 The Authors. *Microscopy Research and Technique* published by Wiley Periodicals LLC.

KEYWORDS

calcified cartilage, comparative histology, growth pattern, mineralization, morphology

1 | INTRODUCTION

The development of the vertebrate skeleton starts in the embryo with differentiation of cartilage from the mesenchymal tissue and advancing in the fetal and post-natal life with a close cartilage–bone relationship and a similar mineral deposition process in mammals metaphyseal growth plates (Pazzaglia, Reguzzoni, Casati, et al., 2020a; Pazzaglia, Reguzzoni, Depero, et al., 2020b). The batoids (Elasmobranchs) calcified cartilage represents a different mineral deposition pattern (Applegate, 1967; Bordat, 1988; Clement, 1992; Egerbacher et al., 2006; Kemp & Westrin, 1979; Seidel, Blumer, Pechriggl, et al., 2017; Seidel, Blumer, Zaslansky, et al., 2017; Takagi et al., 1984). Several histomorphological, ultra-structural imaging and analytical techniques have been applied to study the correlated growth-mineralization process. However, several questions have not yet received so far an exhaustive answer, in particular those concerning: (i) the characteristics of mineral crystal deposits; (ii) the chondrocytes capacity of duplication and survival within the calcifying matrix; (iii) the fluids diffusion in the latter peculiar and confined environment (Dean, Mull, et al., 2009; Dean, Youssefpour, et al., 2009); (iv) the factors determining the crustal versus catenated tiles pattern layout in batoids (Pazzaglia, Reguzzoni, Manconi, et al., 2022; Schaefer & Summers, 2005). To contribute to fill the knowledge gap in this scenario, this study investigates the mineral and histomorphotraits of the batoid *R. asterias* calcified cartilage skeleton vs the teleost *X. gladius* rostral bone and the mammalian *H. sapiens* compact, remodeled bone. *R. asterias* girdles, pterygia and fins radials have been compared with rostral and cortical bone matrix through histology/ histochemistry (a), scanning electron microscopy (SEM) (b), heat-deproteination techniques (c), thermo gravimetric analysis (TGA) (d), differential scanning calorimetry (DSC) (e), and Fourier-transform infrared spectroscopy (FTIR) (f). The elasmobranchs cartilage calcification starts with focal mineral depositions, growing and compacting through individual units of variable outline in the appendicular and body skeleton cartilage, offering matter of study to investigate the mineral deposition and morphofunctional adaptive strategies to mechanical demand on the tissue and the relationship with the locomotion type, the feeding habits and the water column inhabited by these fishes (Pazzaglia et al., 2023). Previous studies focused on the tessellated endoskeleton organization describing the segmental, complex architecture (Dean, Mull, et al., 2009; Maisey et al., 2020; Seidel et al., 2020), the inner mineralized structure of the tesserae (Seidel et al., 2016; Seidel, Blumer, Pechriggl, et al., 2017; Seidel, Blumer, Zaslansky, et al., 2017) and the growth pattern characterized by a scattered distribution in the cartilage of calcified and uncalcified zones (Chaumel et al., 2020). As general rule, the skeletal segments cartilage anlage growth results from a series of bioprocesses shared by all cartilaginous, embryonic tissues, characterized by chondrocyte mitoses, matrix synthesis and extrusion in the pericellular space (Hall, 2007). The elasmobranchs

early mineralized, calcified cartilage scaffold is not a provisional tissue remodeled and replaced by secondary bone, therefore representing the definitive calcified frame of the skeleton.

2 | MATERIALS AND METHODS

2.1 | Preparation of anatomical specimens of *R. asterias*

The calcified cartilage samples were obtained from two, adult specimens of *R. asterias*, Delaroch 1809 (weight female 179 g and male 343 g) caught in a scientific campaign carried out by the DISTAV team (University of Genova) in the Ligurian Sea (North-West Mediterranean). This work was carried out within the fishery Data Collection Framework (DCF) funded by the Italian Ministry of Agriculture, Food and Forestry policies (MIPAAF), at present MASAF (Ministry of Agriculture, Food Sovereignty and Forest), and by the European Commission (EC).

Photographs and x-rays in the dorso-ventral projection of the whole fish (Figure 1a,b) were taken before dissection (within 24 h from the capture). The study-selected skeletal specimens (pectoral, pelvic, tail dorsal fins and girdles) underwent to two different protocols: (1) removal of skin, subcutaneous tissue and main dorsal/ventral muscle layer, then immediately fixed in formaldehyde 10% solution for the histomorphology study; (2) the same three steps, but with a more accurate removal of muscles between the fin rays, then fixed in the same formaldehyde solution for 24 h, washed in distilled water, dehydrated in ethanol and left to dry for heat-deproteination and mineral analyses. Bone samples of teleost *X. gladius*, Linnaeus 1758, rostrum and *H. sapiens*, Linnaeus 1758, cortical diaphysis, obtained by likewise processed and unused specimens in earlier papers (Pazzaglia, Reguzzoni, Casati, et al., 2020a; Pazzaglia, Reguzzoni, Depero, et al., 2020b; Pazzaglia, Reguzzoni, Saroglia, et al., 2022), were used for comparative analysis vs the *R. asterias* calcified cartilage.

2.2 | Heat-deproteination of *R. asterias*, *X. gladius*, and *H. sapiens* calcified matrix specimens

Dry specimens (1 × 0.5 cm) of *R. asterias* fins' radials and 3-mm thick transverse sections of the pterygia or first compound radial (placed on glass slides) were submitted to heat deproteination in a muffle furnace at 400 and 1200°C/24 h. The heated specimens of calcified matrix (*R. asterias*) become brittle and can be easily dissociated in single or grouped calcified units (tesserae or radials' cylindrical tiles). These were repeatedly cleaned ultrasonically in distilled H₂O solutions of NaOH 0.05 M to remove at best the black, organic carbon deposits from the mineral phase, then were dehydrated in increasing concentrated ethanol solutions and mounted dry with a cover slip on glass

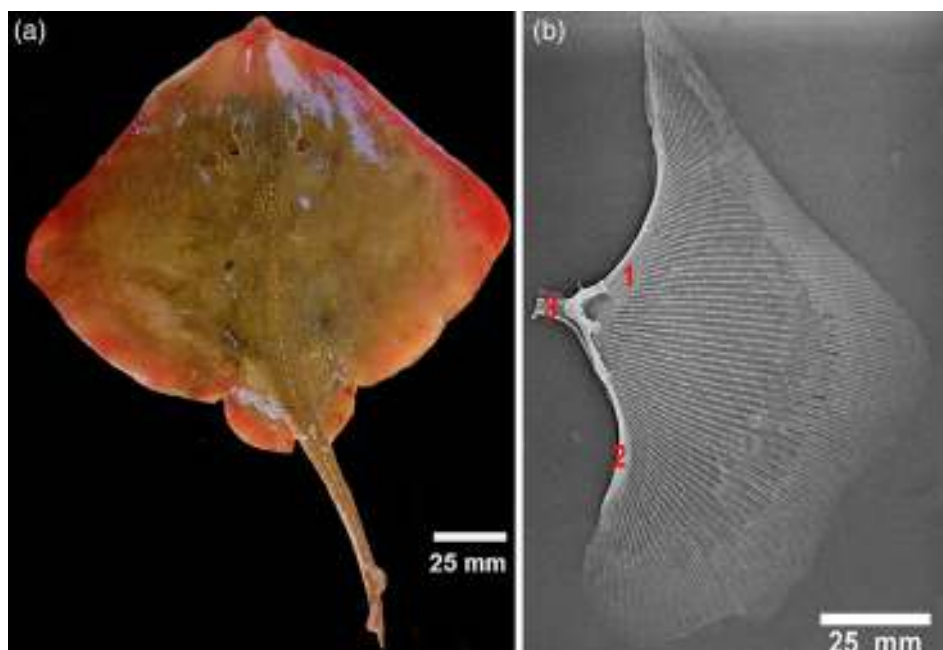


FIGURE 1 (a) Dorsal view of *R. asterias* showing the unbroken skin coating of rostrum, skull, spine and pectoral fins. The pelvic fins are much smaller than the first. The tail is thin, ending with three vertical, dorsal fins. (b) Dorso-ventral x-ray projection of the right pectoral fin showing the segmented propterygium (1), the mesopterygium, the neopterygium, the metapterygium (2) and the sectioned pectoral girdle (3). Full view of the rays fan with the aligned radial segments.

slides to be observed with an Olympus BX51 microscope (Olympus Optical Co., Ltd., Japan). The same chopping and cleaning procedure was carried out on the *X. gladius* rostrum and *H. sapiens* cortical, diaphyseal bone of unused samples of earlier studies (Pazzaglia, Reguzzoni, Casati, et al., 2020a; Pazzaglia, Reguzzoni, Depero, et al., 2020b; Pazzaglia, Reguzzoni, Saroglia, et al., 2022).

2.3 | Scanning electron microscopy of *R. asterias*, *X. gladius*, and *H. sapiens* calcified matrix specimens

Part of the fragmented specimens of calcified cartilage (*R. asterias*) and bone matrix (*X. gladius*, and *H. sapiens*), the latter of size ≈ 2 mm, were critical point dried in CO_2 environment, fixed with bi-adhesive tape on stubs, coated with a thin layer of gold in a sputter-coater (Emitech) and observed with a Philips XL30 Scanning Electron microscope (Philips, Eindhoven, The Netherlands), obtaining EDAX atomic spectra for each specimen class (with the gold peaks removed to avoid superimposition).

2.4 | Mineral analysis of *R. asterias*, *X. gladius*, and *H. sapiens* calcified matrix specimens

Differential scanning calorimetry (DSC) was performed by a Q2000 apparatus (TA Instruments, New Castle, DE, USA) interfaced with a TA5000 data station by heating ≈ 3 mg of powder in an open aluminum crucible from -20°C to 350°C and then cooling down to -20°C (heating and cooling rate = $5^\circ\text{C}/\text{min}$) under nitrogen flux (50 mL min^{-1}). Three independent measurements were acquired on each sample. The temperature accuracy of the instrument is $\pm 0.1^\circ\text{C}$, the precision is $\pm 0.01^\circ\text{C}$, and the calorimetric reproducibility is $\pm 0.05\%$. DSC data were analyzed by the Universal Analysis software by TA Instruments. The thermo-gravimetric curves were acquired by a thermo-gravimetric

analyzer (TGA Q5000, TA Instruments Inc., USA) interfaced with a TA5000 data station by heating about 5 mg of sample in a Pt crucible under N_2 flux (50 mL min^{-1}) from 25 to 1000°C at $10^\circ\text{C}/\text{min}$. The data were analyzed by the Universal Analysis software by TA Instruments, considering also the plot of the derivative of the weight with respect to temperature (DTG curve). Infrared spectra were acquired at room temperature using a Nicolet FTIR iS10 spectrometer (Nicolet, Madison, WI, USA) equipped with Smart iTR with a diamond plate. Thirtytwo scans in the $4000\text{--}600\text{ cm}^{-1}$ range at 4 cm^{-1} resolution were coadded. X-ray powder diffraction analyses were performed by covering a zero background Si sample holder with a thin deposit of powder of the different samples and by acquiring the patterns from 3° to 50° with a D5005 instrument by Bruker (40 kV and 40 mA for the x-ray generation, $\text{Cu K}\alpha$ radiations, 0.02° step size, 10 s counting time).

2.5 | Histomorphology and histochemistry of *R. asterias*

Specimens (3 groups) of pectoral, pelvic, tail dorsal fins and girdle segments, pterygia, and first compound radial were processed by three different protocols:

- Group 1 was decalcified in a solution of acetic-hydrochloric acid (2% $\text{CH}_3\text{COOH}/2\% \text{HCl}$) for 1 week, dehydrated in increasingly concentrated ethanol- H_2O solutions and embedded in paraffin. Transverse and longitudinal sections $10\ \mu\text{m}$ in thickness were serially cut with a sledge microtome and stained with hematoxylin-eosin, trichromic Masson, PAS, Alcian blue and Von Kossa methods. The slides were observed with an Olympus BX 51 microscope (Olympus Ltd., Japan).
- Group 2 was embedded undecalcified in paraffin: only transverse sections were cut and stained with the same methods of Group 1 (including the tail dorsal fins).

- Group 3 (undecalcified, fixed specimens) was embedded in Technovit 7200 resin (Kulzer GmbH) and 150–200 μm thick sections were prepared using the Exact cutting/grinding system (Exact Advanced Technology GmbH) and stained with von Kossa or methylene blue–acid fuchsin. The slides were observed with an Olympus BX51 microscope (Olympus Ltd., Japan).

3 | RESULTS

3.1 | Macro- and micro-layout of fins and girdles endoskeleton of *R. asterias*

The studied batoid is characterized by a flat body with two large right and left pectoral fins connected to the axial skeleton and through the pectoral girdle, but indistinguishable by external observation because covered by an unbroken skin layer on both the dorsal and ventral surface, also extending to include the short rostrum. The smaller pelvic fins are laid in the back on both sides of the tail (Figure 1a). The fins appendicular skeleton is a mechanical system formed by splices (amphiarthroses joints) and stiff segments (radials) providing a variable 3-D flexibility to the whole anatomical structure (macro-scale). The

joints can be distinguished in two types: (i) diarthroses between girdles and pterygia, with a wide 3D range of movement and (ii) amphiarthroses, with a limited freedom of movement in the perpendicular plane to the flat fin surface. The radials (stiff segments) consist of a cylindrical body of uncalcified cartilage stiffened by an inner axis of one or more columns of calcified cartilage tiles (Figure 1b). At micro-scale level, the radials are built up by two phases i.e., the outer uncalcified cartilage muff and the inner columns of aligned, calcified units (tiles). Moreover, a further element adds mechanical complexity to this hierarchical structure at tissue level, i.e. scattered focal zones of uncalcified matrix inside the calcified cartilage, whose presence is basic to explain the growth processes of this cartilaginous tissue (Pazzaglia et al., 2023; Pazzaglia, Reguzzoni, Saroglia, et al., 2022).

3.2 | Heat-deproteination imaging of *R. asterias*, *X. gladius*, and *H. sapiens*

Heating at 400°C specimens of *R. asterias* endo- and appendicular-skeleton cause organic matrix combustion leaving black, carbon deposits between the mineral aggregates, allowing to document at low microscopic magnification shape and structural layout of radials

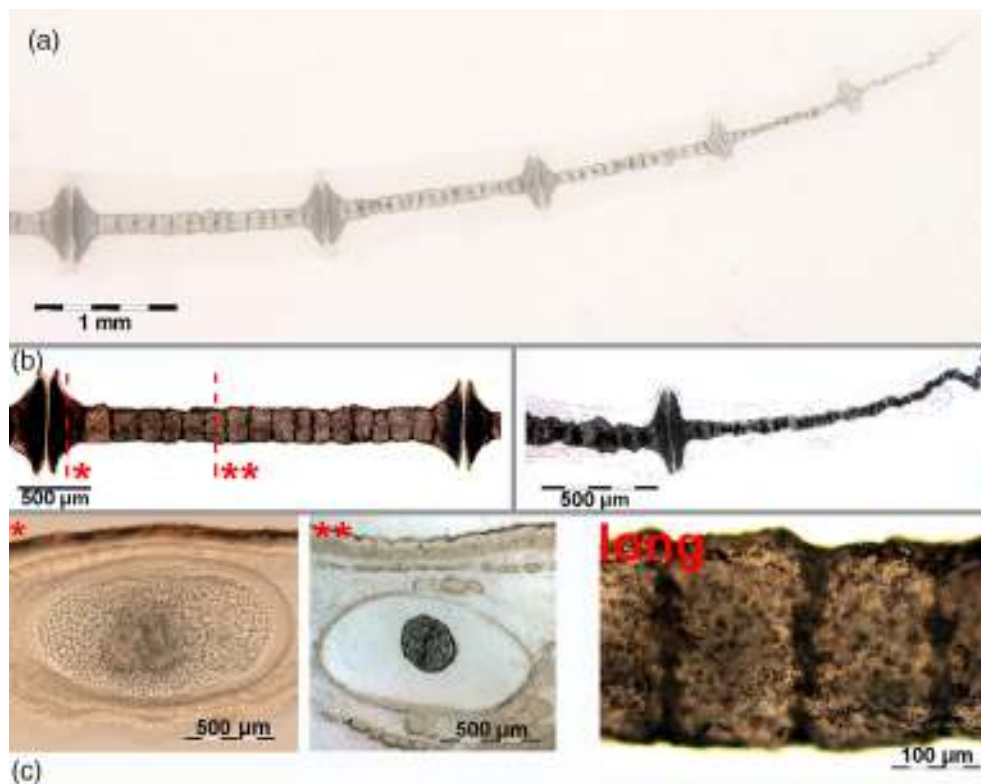


FIGURE 2 Undecalcified, heat-deproteinated radials in transmitted light. (a) Ray apical zone showing the aligned radials with the inter-radial joints (amphiarthroses) and the calcified central column formed by cylindrical tiles with enlarged joint disks at the extremities. (b) First line (medial) and most apical (lateral) radials showing the regular tiles shape/size and alignment of the first, the smaller size and irregular calcification centers of the apical (dotted lines and asterisks correspond to the transverse trans-illumination sections of (c)). (c) * Unstained transverse sections in transmitted light show the oval shape of the calcified cartilage disk and the thinner, flaring border allowing to distinguish the regular chondrocyte lacunae distribution in the intercellular calcified matrix. The darker calcified central area corresponding to calcified matrix increased thickness of the central zone. ** Unstained transverse section showing the central column calcified matrix surrounded encircled by an uncalcified cartilage muff of oval shape. Long: Higher magnification of column longitudinal section documenting the carbon deposits (black) between adjacent tiles and calcified cartilage matrix wrapping up chondrocyte lacunae.

and pterygia mineralized tiles (Figure 2a,b). Repeated ultrasonically polishing steps in weak NaOH solutions can partially clean the most superficial carbon deposits but leaving those encapsulated within the chondrocyte lacunae and the smaller residuals embedded into the inorganic phase producing a gray coloration of the tile columns when these are observed in trans-illumination (Figure 2c**/long). This has allowed to document the radials length and diameter increment from the lateral fin edge to the medial zone articulating with the pterygium (Figure 3a). On the contrary, the mean tile number among radials calcified column does not show significant differences between the medial and lateral fin zone, but excluding the most apical radials where the tiles number is not assessable (Figure 2b). These data have provided a reliable evidence that radials length growth develops at level of the single tile calcification center (Pazzaglia et al., 2023).

The heated radials, pterygia and compound radial segments were brittle and single tiles could be easily separated by gently manipulation, distinguishing the endoskeletal tesserae for their polygonal perimeter by the tiles of the columns, whose outline varies from cylindrical to tripolar (Figures 3a and 4a-c). These divergent outlines are

related to two distinct patterns of mineral deposition, already reported as crustal and catenated mineral deposition (Pazzaglia, Reguzzoni, Manconi, et al., 2022; Schaefer & Summers, 2005). Heating at 1200°C produced a thermal conversion of β -tricalcium phosphate to crystalline hydroxyapatite, with a complete disappearance of carbon deposits and crystals' compaction of tesserae and cylindrical radials' tiles, size reduction but unchanged outline (Figure 4d).

Otherwise, 400°C heated samples of *X. gladius* rostrum and *H. sapiens* cortical bone were harder and most compact than that of *R. asterias*. The same chopping procedure (carried out in ceramic mortar) does not allow to separate subunits at level of lamellae or osteons (Figure 3d,e). These bone samples observed in trans-illumination have a gray coloration of different density due to the irregular thickness (Figure 3d) and birefringence in polarized light suggesting a lamellar, subperiosteal layout (Figure 3e). Also osteocyte lacunae can be observed in the compact, calcified mass (Figure 3d,e), however subunits discrimination between laminae and osteons is structurally undistinguishable at this low magnification. SEM associated with EDAX analysis of the same heated specimens confirms a more compact

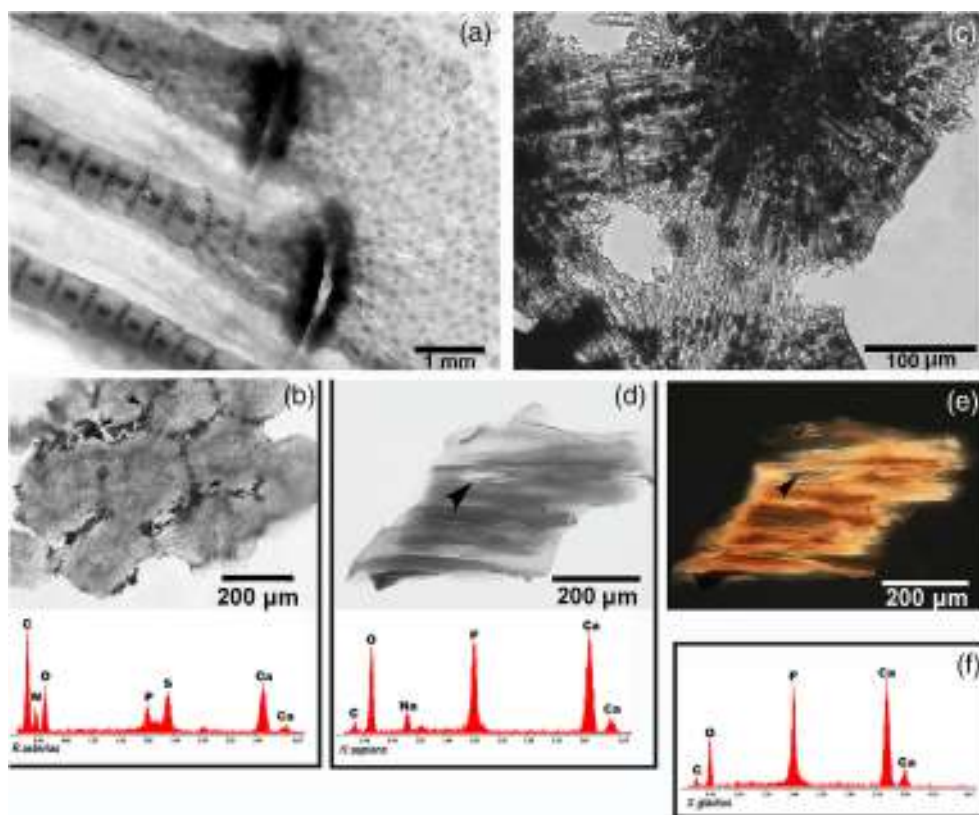
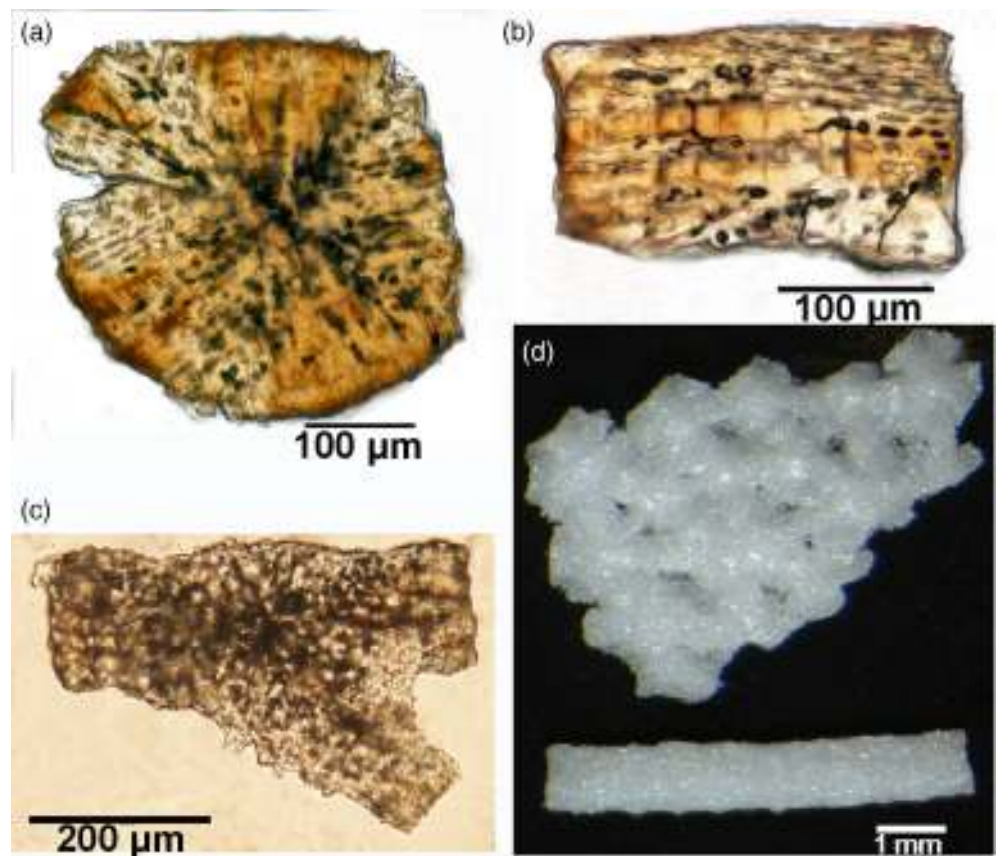


FIGURE 3 Heat-deproteinated trans-illumination samples and EDAX analysis. (a) (*R. asterias*) Transition zone between the pterygia external border and the first line of radials evidencing the unit shape and architecture of the first tissue (right) and the radials' columns (left). (b) (*R. asterias*) Higher magnification of pterygia tissue shows a flooring of polygonal tesserae and the uncalcified cartilage carbon deposits in interspaces between tesserae. Calcified cartilage EDAX spectrum with two Ca peaks and C, N peaks. (c) (*R. asterias*) Higher magnification of inter-tesseral connections through needle-like mineral deposits whose shape has been conditioned by chondrocytes alignment. The linking tissue is brittle and easily fractured (arrow). (d) (*H. sapiens*) Split bone samples in trans-illumination showing a compact calcified matrix texture and an osteocyte lacuna inside (arrow). Bone EDAX spectrum with two Ca peaks, no C, N peaks. (e) (*H. sapiens*) Same specimen of D observed in polarized light showing the collagen fibrils parallel texture birefringency. (f) (*X. gladius*) Rostral bone (teleost) EDAX spectrum showing the same peaks of D.

FIGURE 4 Calcified cartilage tiles of *R. asterias* heated at 400°C. (a–c) Tile shape of axial and appendicular skeleton: A polygonal (axial skeleton, pterygia); (b, c) cylindrical (appendicular skeleton radial columns). (d) Calcified cartilage polygonal/column tiles, heated at 1200°C undergoing to size and weight reduction and hydroxyapatite crystal transformation.



texture of *H. sapiens* and *X. gladius* calcified matrix than that of *R. asterias*. The EDAX spectra show in the *H. sapiens* and *X. gladius* spectra (Figure 3d,f) only the Calcium and Phosphorus peaks, while in the *R. asterias* also the Carbon peak is evident (Figure 3b).

3.3 | Physicochemical characterization of *R. asterias*, *X. gladius*, and *H. sapiens*

The comparative TGA, XRPD graphics and IR spectra of *H. sapiens*, *X. gladius*, and *R. asterias* calcified skeletal matrices are respectively shown in Figures 5a–f, 6, and 7a–c, while the detailed description (including references) are reported in the attached Supplementary Material S1.

3.4 | Histomorphology and histochemistry of *R. asterias*

Endo- and appendicular-skeleton undecalcified histology confirmed the growth pattern through multiple and discrete mineralization centers already shown by heat-deproteination. The differences between the two skeletal sectors were characterized by the position of the initial mineral deposits, peripheral or “crustal” in the first (Figure 8a), central or “catenated” in the second (Figure 10a) and by the further growth pattern leading to the segments full-developed layout

(Figure 10b–d). In the endo-skeleton (rostrum, neuro-cranium, synarcuals, and girdles), but also in the largest appendicular-skeleton segments (pterygia, compound radials, and tail dorsal fins) the earlier, discrete mineral deposits appear below the cartilage anlage outer borderline, but leaving a superficial thin layer of uncalcified tissue (Figure 8 A,B). The peripheral calcifications are discontinuous and irregular, often showing transverse fissures due to the tensional stress force developed by the growing central, uncalcified cartilage mass (Figure 8b). Observation of a more advanced developmental stage documents that mineral deposits expand both outwardly and inwardly, at first without a complete fusion between the single calcified units (Figure 9a), then forming a flooring of polygonal tesserae on the surface (Figure 9a,b). In the transverse sections, the outer calcified layer takes variable morpho shapes, that is (i) single, large-base cones; (ii) single rectangular blocks, and (iii) blocks with basal fusion between neighboring tiles or with a complete fusion forming tracts of an unbroken, calcified layer (Figure 9a,c,d). Mineral deposits have never been observed in the cartilage central zone, where chondrocytes show a higher zonal duplication rate documented by cell isogenic groups formation (Figure 9a). Distinctive features characterize the cell morphology of the tesserae, ranging from nucleated chondrocytes embedded into the calcified matrix to empty lacunae and scattered uncalcified matrix zones within the mineralized mass (Figure 9b,c).

In the appendicular-skeleton pectoral, pelvic, and tail dorsal radial fins (Figure 10a), the initial mineral deposition was central (Figure 10e) progressing either eccentrically and along the radial longitudinal axis

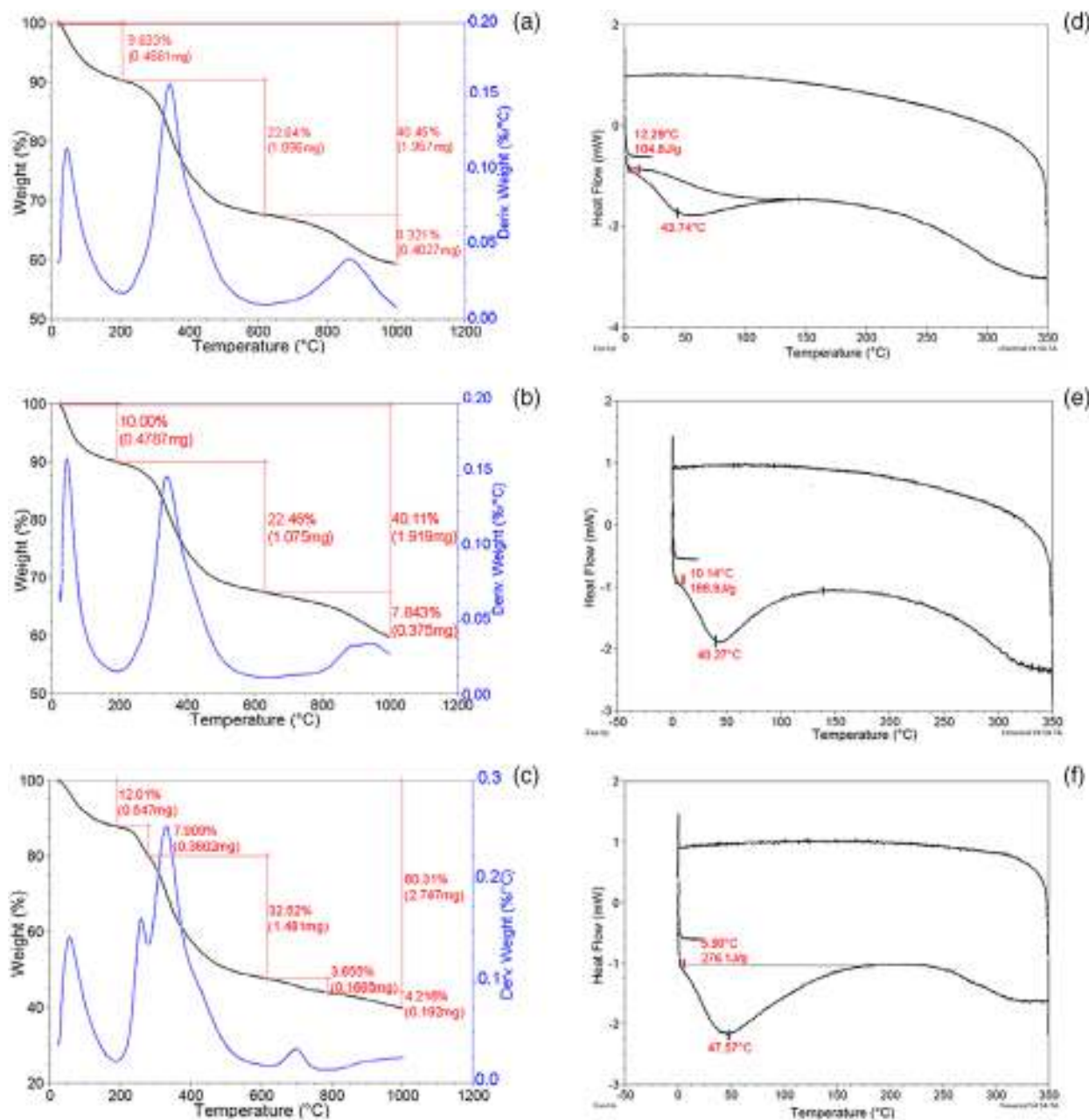


FIGURE 5 Thermo-gravimetric analysis (TGA and DSC) graphs of *H. sapiens* bone (a, d), *X. gladius* bone (b, e), and *R. asterias* calcified cartilage (c, f) detailed in Section 3.3.

(Figure 10b-d). The radial length increment was due to the growth of each aligned tile (Figure 10d). The columns layout ranged from mono- to multi-columnar. The tail fin radials as well as those of pectoral fin lateral zone were mono-columnar, while radials were bi-columnar in the medial zone and longer and multi-columnar in the pelvic fins (Pazzaglia, Reguzzoni, Manconi, et al., 2022). The heat-deproteinated samples of separated tesserae or cylindrical tiles showed a chondrocytes lacunae alignment with a radial pattern in the former and longitudinal in the latter (Figure 4a,b). Nucleated chondrocytes filled the lacunae either in the calcified and uncalcified matrix (Figures 8b,c and 10f).

Histochemistry (focusing on paraffin-embedded, undecalcified pectoral and tail fin radials) did not give legible results in the calcified zones because the mineral phase deposits altered the color intensity of each specific staining. Therefore, only uncalcified cartilage zones have been used for comparative histochemical analysis selecting the outer muffle of pectoral fin mono-columnar radials. As documented in a previous study (Pazzaglia et al., 2023), mineral deposition formed a loose calcified fibers felt leaving large spaces in the 3D network filled by organic phase molecules. Therefore, the staining results in the uncalcified matrix surrounding the column can be extrapolated to

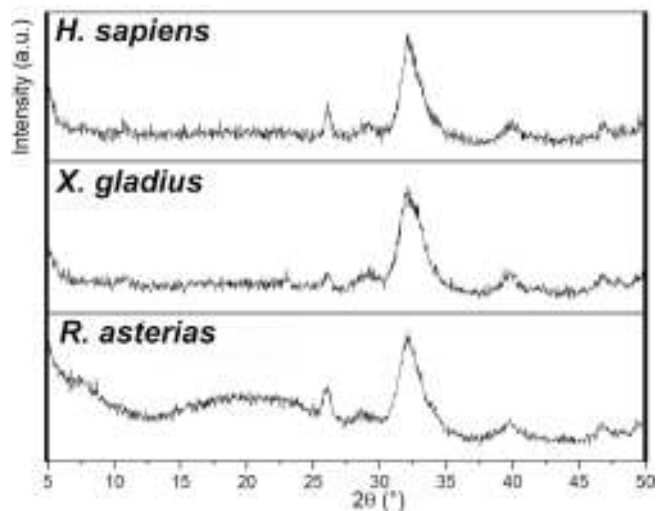


FIGURE 6 XRD pattern and size particles analysis of *H. sapiens* bone (a), *X. gladius* bone (b) and *R. asterias* calcified cartilage (c) detailed in Section 3.3.

the no-collagenic organic phase components of the nearby calcified matrix of the column tiles. The different stain intensity of Masson trichrome, Alcian blue, and PAS (Figure 8d–f) between the matrix around the chondrocytes isogenic groups (#) and the inter-territorial matrix (*) was clearly distinguishable, yet documenting only large scale variations the tissue component amount, for example, collagen, proteoglycans, and glycosaminoglycans (Table 1). High magnification images of impending calcification zones of *R. asterias* calcifying skeleton showed hypertrophic chondrocytes undergoing embedding into the mineralized matrix (Figure 8c) suggesting a relationship between cell hypertrophy and H₂O/ions transport at the cell membrane level as in the mammalian metaphyseal growth plate cartilage (Pazzaglia, Reguzzoni, Casati, et al., 2020a). The tail dorsal fins showed a mixed skeletal structure combining the radial pattern with a set of more flexible keratin, long rods (Figure 10a–c). The radials were mono-columnar with thinner and slender tiles than that of the pectoral fins (Figure 10d) but otherwise with the same traits and layout of calcified-uncalcified texture (Figure 10e,f).

Calcified cartilage in *H. sapiens* skeleton is present particularly in the fetal and post-natal growth period (in the bones cartilage anlagen ossification centers or in the metaphyseal growth plate cartilages respectively), therefore only histological and SEM techniques are enforceable to a comparative study due to the need to part calcified cartilage from bone matrix in the mineral analysis techniques. From the material of an earlier study on endochondral ossification (Pazzaglia et al., 2018) it is possible to document the mineralized cartilage serving as scaffold to the apposition of the first bone matrix layer by the periosteum (Figure 11a–c). The earlier cartilage mineral deposits with a globular outline were not present inside the chondrocytes lacunae and undistinguishable from those of the bone matrix, both showing a trend to coalescence and formation of solid plaques (Figure 11d,e).

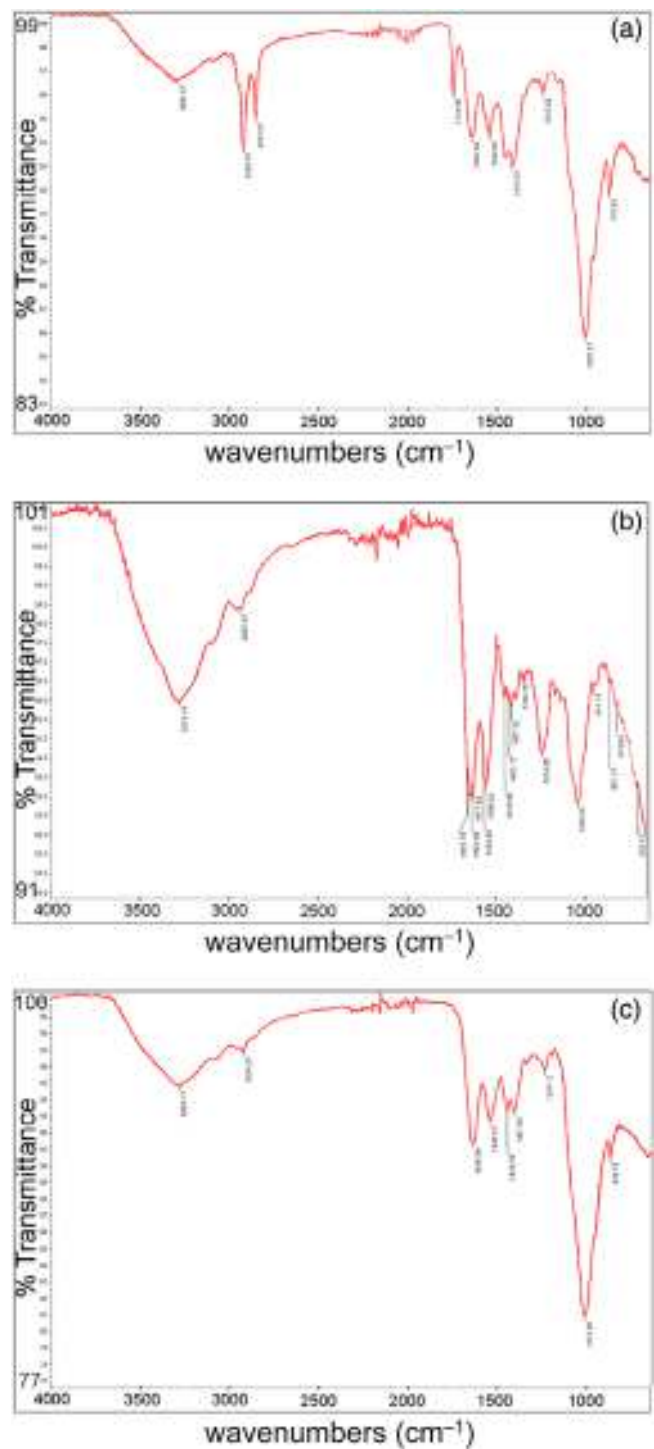


FIGURE 7 FTIR spectra of *H. sapiens* bone (a), *X. gladius* bone (b) and *R. asterias* calcified cartilage (c) detailed in Section 3.3.

4 | DISCUSSION

Outline, size and texture of the cartilage skeletal models or anlagen starts by chondrocytes differentiation, proliferation and cartilage matrix synthesis, while the further development is characterized by a series of transformations: (i) CaPO₄ nucleation in the cartilage model;

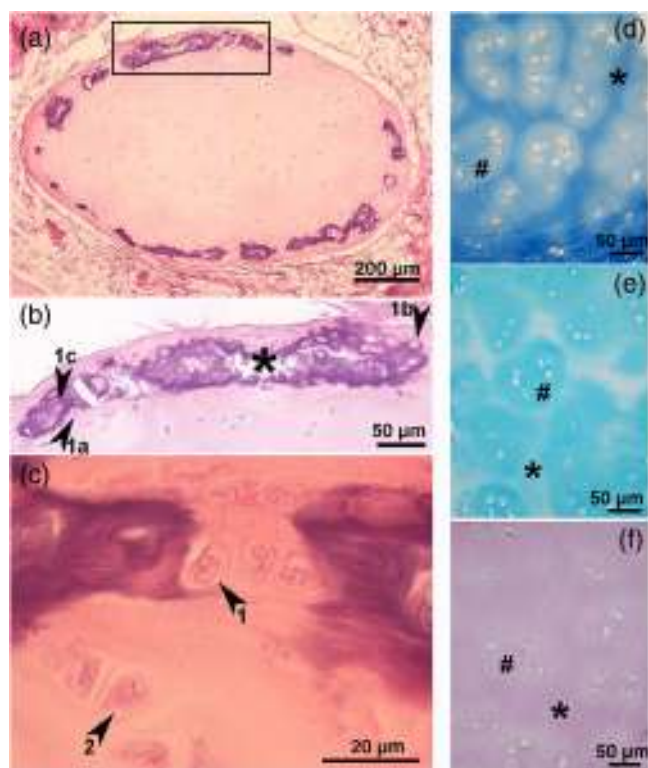


FIGURE 8 *R. asterias* calcifying cartilage earlier mineral deposition stage and histochemistry. (a) Hematoxylin-eosin transverse section pelvic compound radial. Focal and marginal mineral deposition in cartilage matrix showing a fusion trend of single foci (crustal calcification pattern). (b) Hematoxylin-eosin, detail of A outlined area. Chondrocytes in progressing phases of cell embedding into the calcified matrix: 1a, 1b, 1c. The tears in the calcified matrix (*) are due to the model growth process of the uncalcified matrix core. (c) Hematoxylin-eosin. (e) Enlarged cartilage lacunae in the process of being embedded into calcified matrix. However, also chondrocytes nearby the calcification site show globular shape, enlarged/swollen cytoplasm. (d-f) Masson-trichromic, Alcian blue, PAS. The mineralized matrix is not usable for histochemistry staining due to the hardening superimposition effect of inorganic phase, however in the un-mineralized matrix the applied staining methods reveal specific stain saturation around chondrocytes isogenic groups (arrows) reported in Table 1. * and # correspond to the histological fields of Figure 8 (d), (e), (f).

(ii) vascular invasion; (iii), osteoblasts differentiation followed by osteogenesis and remodeling. Two main patterns of skeleton development can be distinguished in the sub-phylum vertebrata, that is, the endochondral ossification model, where the calcified cartilage is gradually replaced by bone matrix and the elasmobranchs persistent calcified cartilage model, where the fetal calcified tissue continues to grow throughout the whole life span. The first is the most diffuse model among the vertebrate species, the second is restricted to the cartilaginous fishes of the Class Chondrichthyes. The bone and calcified cartilage hierarchical structure (both tissues consisting of an organic and inorganic phase) characterizes the hardness/stiffness of the respective skeletal segments, while the fins or limbs morph/pliability/joints

articulation have developed through an evolutive path (Tanaka & Tickle, 2007) selecting the more favorable adaptation to the environment where the species live and move.

The aim of this study is a comparative analysis of the growth/calcification patterns between a mammalian (*H. sapiens*), a teleost fish (*X. gladius*) and a chondrichthyan fish (*R. asterias*) carried out through macro-structure, histomorphology/histochemistry, heat-deproteination, SEM, thermo-gravimetric, and x-rays diffraction analyses. The species and the skeleton specimens have been selected on the basis of their locomotion respectively on the ground (*H. sapiens*, limbs cortical bone) and in the water column (*R. asterias*, fin radials, respectively). The third teleost fish (*X. gladius*, rostral bone) has been included to get a bone specimen of sufficient size to be comparable with mammals cortical bone. Likewise, mammals calcifying cartilage samples can be only obtained from the metaphyseal growth plate in small amounts of tissue (further reduced by the need to clean cartilage from the bone matrix layer deposited by osteoblasts on the inter-columnar septa) therefore an insufficient quantity to perform a comparative mineral analysis. The material of an earlier study carried out with histomorphology combined with heat-deproteination/SEM imaging on *H. sapiens* fetal metacarpals growth plate cartilages has provided usable images of early calcification morphology for comparison with the chondrichthyes calcified cartilages (Pazzaglia et al., 2018).

The mechanical implications of calcification in skeletal segments development, growth and repair of living organisms have been matter of a large number of studies and researches since the mineral deposition in the biological matrices extends from the Vertebrata to the simplest living organisms as Metazoan Porifera. On the basic assumption that the mineral deposition serves to stiffen a mobile segment (as any other part of the skeleton, alone or in combination with the organic fibers texture) in relation to weight bearing or movement compressive/tensional stress loads, a *skeletal mechanostat* theory has been suggested by Frost (1995a, 1995b, 1996) based on a negative feedback regulation. However, this multiform articulation (Supplementary Material S2) sets doubts on the possibility to formulate an inclusive, general *skeletal-biologic paradigm (mechanostat)* according to the Frost's terminology. Certainly, the mammalian tetrapods limbs, homologous to the chondrichthyes fins as extensively documented by the transformation of fins into limbs (Hall, 2007) fit with the higher weight-bearing demand and performance due to the force of gravity on the ground than that of the Batoidea calcified cartilage in the water column. However, it is difficult to explain this transformation exclusively in the ontogeny sphere with a mechanical feed-back model or living calcified tissues and systems adaptation to the mechanical performance through the growth process (Nyman et al., 2005) as well as to integrate the polyphosphate biochemistry with the crystal nucleation theory (Omelon et al., 2013). As a matter of fact, this transformation cannot be explained without consideration of the complex and long evolutionary path which involves the regulation of the HoxD genes expression and the related signaling factors (Fgfs, Wnt, Tbx) in the development of the fins and the limbs

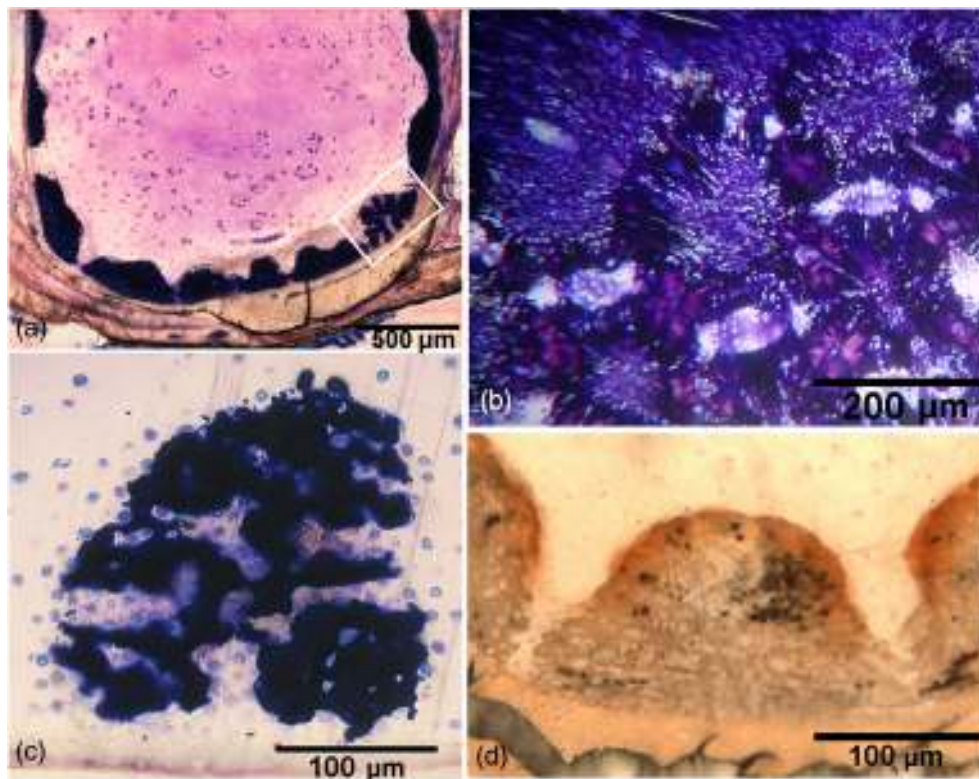


FIGURE 9 *R. asterias* calcifying cartilage late mineral deposition and growing phases. (a) Toluidine blue, transverse section, pelvic compound radial. Different growth, calcification and aggregation patterns of calcified tesseral units and chondrocytes isogenic groups distribution in the central, un-calcified cartilage core. (b) Toluidine blue, superficial tangential section, pelvic compound radial. Polygonal tesserae bridged through calcified cartilage connections (dark blue stain). The tesseral central body shows a higher density of cellular lacunae than in the bridging links. Chondrocytes are aligned forming radial rows. Scattered, uncalcified matrix zones can be observed in the mineralized tissue mass. (c) Toluidine blue, transverse section, detail of A outlined area. Tesseral unit still in an active growth phase, evidenced by uncalcified cartilage branches with high chondrocyte density. (d) Von Kossa, transverse section. Tesseral unit in less active growth phase, but still evident cell alignment inside the mineralized matrix.

(Tanaka & Tickle, 2007), the chondrogenesis and osteogenesis (Witten & Huysseune, 2007), and altogether the endochondral ossification process (Farnum, 2007).

In mammals bony skeleton three distinct ossification patterns can be distinguished, that is, (1) endochondral, characterized by bone matrix deposition on an already calcified cartilage scaffold as can be observed in the fetal ossification centers and in the post-natal metaphyseal growth plate cartilage development up to the puberty; (2) appositional, with periosteal osteoblasts depositing the new matrix on pre-calcified bone layers of periosteum or within the inner Haver's canals surface); (3) interstitial, with bone matrix extrusion in the inter-cellular spaces between osteoblasts followed by calcification. The first pattern (inside the still uncalcified, cartilage model of the skeletal segment) forms distinct endochondral ossification centers or "nuclei" whose distribution, morph, position and growth lead to the final bone shape. A further major point in mammals bones is that chondrocytes proliferation rate reduction in the ossification centers leads to a gradual slowdown and arrest of the bone size increase (after the puberty in terrestrial tetrapods). Therefore, the fate of the calcifying cartilage in the mammals class is to be reabsorbed and replaced by osteoblasts' bone matrix through the remodeling process: indeed

few traces of the metaphyseal growth plate cartilage longitudinal septa can be still observed within the cortical bone below the metaphysis, but any evidence of them disappears in the diaphyseal cortex (Pazzaglia, Reguzzoni, Casati, et al., 2020a; Pazzaglia, Reguzzoni, Depero, et al., 2020b). The bone appositional/interstitial activity (second and third patterns) is on the contrary maintained along the whole animal life span in the balanced, Haversian remodeling or when stimulated by bone traumatic lesions. For what concerns the *H. sapiens* cortical bone—*X. gladius* rostral bone comparison, the latter samples have been envisaged because they provide sufficient material for a complete, comparative mineral analysis. Indeed, the over-grown anterior segment of the sword fish upper jaw (rostrum) shows a primary osteons texture but without the typical lamellar pattern of the mammals remodeled cortex as shown by circularly polarized light microscopy (Pazzaglia, Reguzzoni, Saroglia, et al., 2022).

The chondrichthyan skeletal mineralization deserves to emphasize two main, specific differences: (1) the calcified cartilage is a permanent tissue not undergoing to the highly regulated process of the mammals growth plate cell-cell interactions (Hall, 2013) and without an arrest after the early growth phase; (2) the skeletal segments growth and the mineral deposition progression depend on a

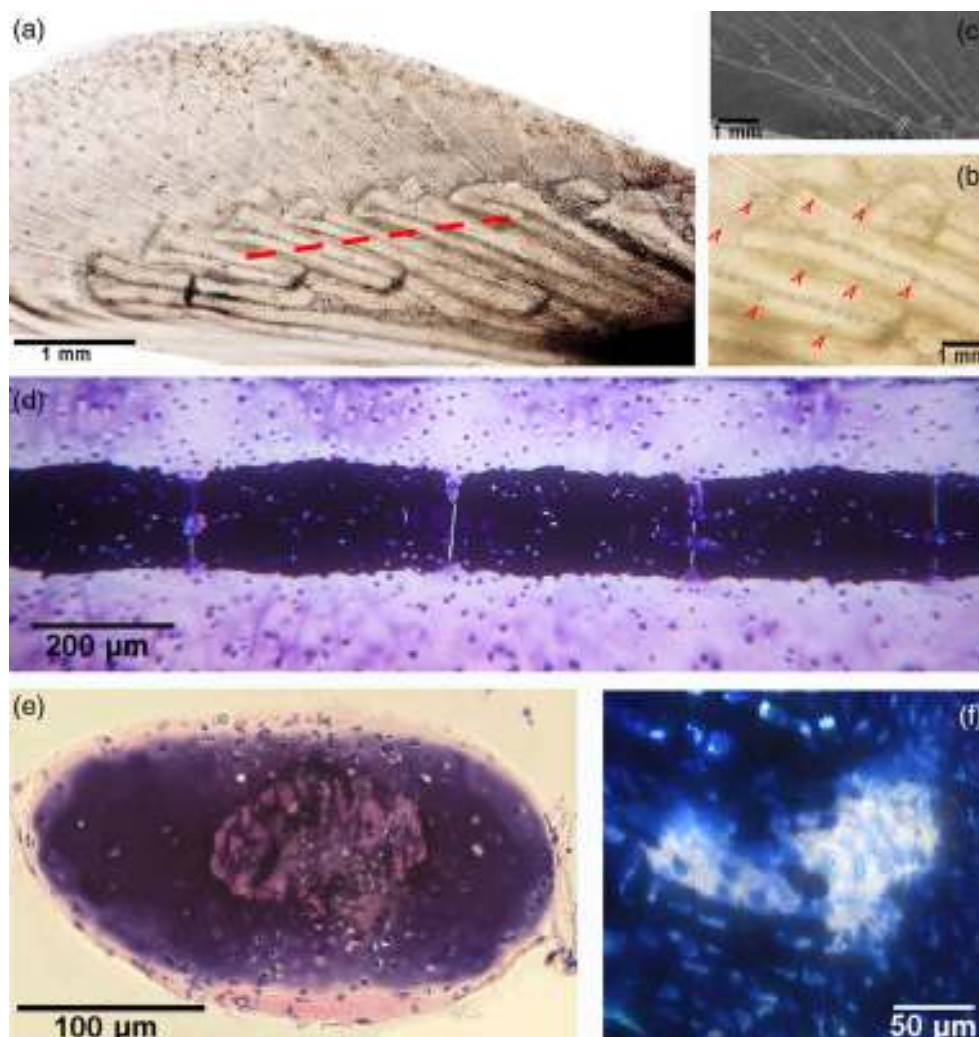


FIGURE 10 *R. asterias*, dorsal tail fin. (a) Trans-illumination image of the whole fin flat surface, revealing the compound layout with a basal series of radials (same structure of fins radials) and a peripheral sector forming a fan of thin and long keratin rods. (b) Trans-illumination at higher magnification documenting the radial structure with a central column of calcified cartilage tiles, surrounded by an un-calcified cartilage muff. (c) Fin x-rays documenting the typical structure of radials with a central column and enlarged disks at the extremities corresponding to the inter-radial joints. (d) Toluidine blue, longitudinal section. The aligned cylindrical tiles of the column are higher than those of the pectoral fins but with the same layout with a thin fissure of uncalcified matrix allowing to distinguish the single units. (e) Toluidine blue, transverse section. Tile oval shape with the major axis parallel to the a-p tail axis. Mineralized cartilage matrix forms the tile central core surrounded by the muff of un-calcified cartilage. (f) Toluidine blue, transverse section. Scarred areas of un-calcified matrix are scattered in the tissue. Also nucleated chondrocytes can be observed into the mineralized matrix.

TABLE 1 Specific density of histochemistry staining around isogenic chondrocytes zones and inter-territorial zones between isogenic groups.

Figure 8	Staining methods	Chondrocytes isogenic zone #	Inter-territorial matrix between isogenic chondrocytes groups*
D	Masson trichromic	+	+++
E	Alcian Blue	+++	+
F	PAS	+	++

Note: * and # correspond to the histological fields of Figure 8 (d) (e) (f).

continuous chondrocytes mitotic activity and mineral deposition. Moreover, both the latter processes are distributed among a large number of calcifying units (endo-skeleton tesseræ and appendicular-skeleton cylindrical tiles) rather than to be gathered at level of two

single sites, the long bone proximal and distal metaphyseal cartilages of mammals. These differences rouse the interest of morphologists and biologists because they represent a modified and simplest skeletal segments growth pattern than the more diffuse endochondral

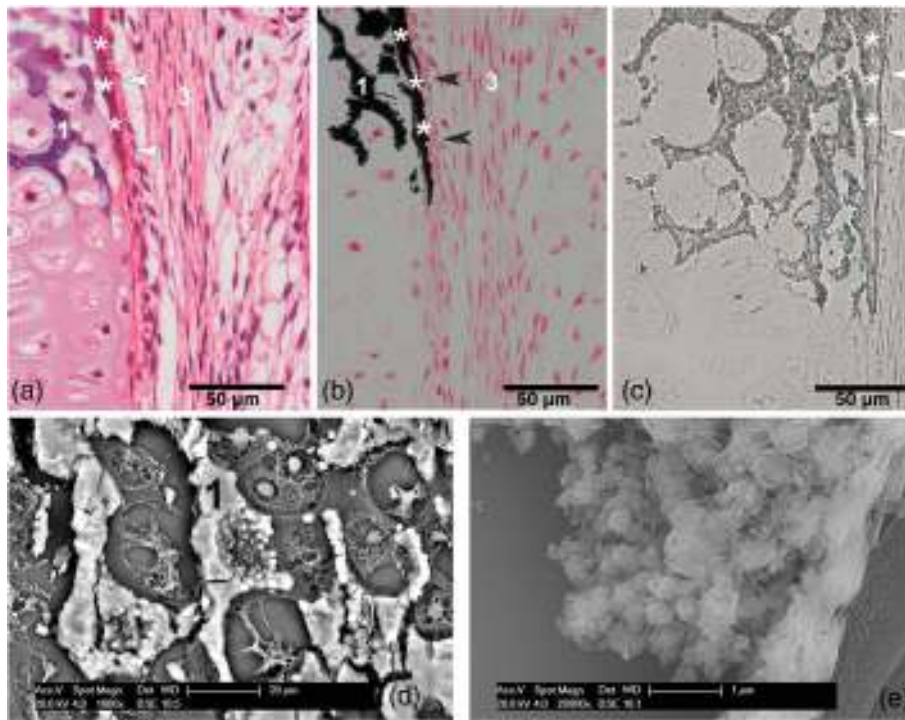


FIGURE 11 *H. sapiens*, metaphyseal growth plate mineralized cartilage. (a) Hematoxylin–eosin, longitudinal section. Mineral deposition on the cartilage matrix at level of the hypertrophic chondrocytes intercolumnar septa (1). A thin layer of mineralized bone matrix has been deposited by the periosteal osteoblasts (*). On the right side is evident the fibrous periosteum (3). (b) (Von Kossa–neutral red, same sections series of (a)). The method stains black both the mineral deposits on the cartilage and that of periosteal bone matrix (1, *). However, the mineral nucleation mechanism is different, being the first controlled by hypertrophic chondrocytes and the second by periosteal osteoblasts (arrows). (c) (SEM/heat-deproteinated slide, same section series of (a)). The early mineral deposits have a globular shape, undistinguishable between cartilage (1) and bone matrix (*). (d) (SEM/heat-deproteinated slide, same section series of (a)). Globular mineral deposits of different size (from about 0.1 to 1 μm) showing a trend to coalescence and formation of solid plaques (1). Mineral deposition occurs only on bone or cartilage matrix, while it has never been observed inside hypertrophic chondrocyte lacunae. (e) (SEM/heat-deproteinated slide, same section series of (a)). Higher magnification confirms the size variations of globular deposits and the trend to coalescence, but reveals a surface roughness which could suggest an earlier level of crystals needle-like pattern. (Images (a) (b) (c) (d) (e) reproduced from Pazzaglia, Reguzzoni, Pagani et al, *Anatomical Records* (2018), 301: 571–580. Open access article distributed under the terms of the Creative Common CC, which permits unrestricted reproduction provided origin properly cited.)

ossification model. As a matter of fact, it can progress without highly regulated cell–cell interactions as osteoclastic resorption, vascular invasion and osteoblasts differentiation (osteogenesis and remodeling) and at the same time it is capable to develop joints with a wide range of movement like the diarthroses between girdles and fins pterygia (Pazzaglia, Reguzzoni, Saroglia, et al., 2022).

Considering cartilage versus bone (organic phase), it is distinguished by the osteoblasts or chondroblasts synthesis of collagen type 1 and type 2, respectively, together with a variety of other organic phase components. At micro-structural level the two collagen types correspond to a different texture layout, with densely packed, parallel oriented fibrils in collagen type 1, whose ordered layout has been set by the synchronous apposition of the osteoblasts sheet below the periosteum and the endosteum forming the respective lamellar systems or circularly inside the Havers' canals, forming the osteons secondary remodeled system (Pazzaglia et al., 2010). The looser 3-D network of type 2 collagen calcified fibers, as recently documented in the batoid *T. marmorata* (Pazzaglia et al., 2023), leaves unmineralized

spaces filled by a variety of organic matrix components, partially characterized in this study by histochemical staining. The osteoid border between the active osteoblasts and the calcification front (well documented in the osteogenesis process with un-decalcified, Von Kossa stained sections) provides an unquestionable evidence that organic phase synthesis precedes mineral deposition. No such clear, histological evidence has been so far obtained in the calcified cartilage skeleton. However, the heat-deproteination method applied in this study supports the last statement validity also for the batoid skeleton mineral deposition owing to the presence of carbon deposits inside or between the mineralized tile units.

Considering cartilage versus bone (organic phase), the basal chemical condition in a saline water solution (but extendable to biological matrices and tissues) for precipitation of CaPO_4 is to reach the saturation point of Ca^{2+} and PO_4^{3-} ions. This study data suggest that either in chondrichthyes skeleton and mammals growth plate cartilage the first mineral deposition occurs through a membrane H_2O and ions transport from the extracellular matrix into the chondrocyte

cytoplasm, reaching in this way the critical Ca^{2+} and PO_4^{3-} concentration in the extra-cellular matrix. This mechanism is also coherent with the growth plate calcification pattern (Maroudas, 1976; Pazzaglia, Reguzzoni, Depero, et al., 2020b; Pazzaglia, Reguzzoni, Casati, et al., 2020a). In the batoid calcifying cartilage, columns of enlarged chondrocytes can be also observed, yet with less cell cytoplasmic swelling than in the growth plate cartilage cells and a compatible condition with living cells. Therefore, these observations do not clash with the hypothesis of a similar mineral deposition pattern but leaving the chondrocytes alive because the Batoid partially calcified skeleton is a permanent tissue, whereas the growth plate calcified cartilage (with its hypertrophic chondrocytes) is provisional and bound to be reabsorbed and replaced by bone in a short time interval.

For what concerns mammals bone matrix, the thickness of the osteoid border below the osteoblasts sheet reveals a time lag between the tropocollagen extrusion from the cell, the fibrils layout organization and the mineral deposition, suggesting a different mineralization pattern from that of cartilage matrix. Assuming that the cell membrane mineral ions concentration mechanisms (H_2O or polar ions transport through the membrane) would be the same in the two cell types, the different histomorphology of the tissue biomineralization can only be explained by the kind of not-collagenic organic phase molecules or the collagen type, acting as nucleating factors of the mineral deposition (Anderson, 1989; Bonucci, 2013; Fleish & Neuman, 1961; Glimcher, 1989, Zeiger et al., 2011). The high number of not-collagenic organic phase elements can explain how it has not been possible so far to formulate a unified theory of the biomineralization process. Posner (1987) has suggested three categories of hypotheses how the cells can promote, regulate or inhibit the process, that is, (i) local rise of inorganic ions concentration; (ii) factors promoting calcification through creation of nucleation sites; and (iii) removal of calcification inhibitors (Bonucci, 2007).

The thermo-gravimetric curves of the inorganic phase matrices compared in the study have documented three mass loss steps corresponding in sequence to water release, collagen decomposition and carbonate decomposition (Biancolillo et al., 2019) with a very similar graphic profile between *H. sapiens* and *X. gladius* bone specimens, while in *R. asterias* calcified cartilage the carbonate decomposition starts at the same temperature of the former and in a wide interval not ending at 1000°C . The three TGA peaks, as evidenced also by the DTG curves correspond to the main mass loss steps, that is, the first ($25\text{--}200^\circ\text{C}$) due to water release, the second ($200\text{--}600^\circ\text{C}$) to collagen decomposition, and the third ($600\text{--}1000^\circ\text{C}$) to crystalline transformation. These mineralogical data fit with the results of a study carried out on human bone osteons carried out with Polarized Raman Spectroscopy. The *H. sapiens* and *X. gladius* bone mineralogical characters are very similar, while differences appear in *R. asterias* calcified cartilage with a second step composed by two processes and a third step with a low mass loss process not ending at 1000°C . The behavior evidenced by TGA is confirmed by DSC and XRD patterns showing the lower crystalline degree and more amorphous material of the calcified cartilage bio-apatite (Patonai et al., 2013; Thompson et al., 2009). Concerning the IR spectra, they also shows the calcified cartilage early

reported differences associated to an important presence of collagen and water (Benedicto de Campos et al., 2011) as testified by TGA measurements.

5 | CONCLUSIVE REMARKS

The combined mineralogical/histomorphological approach to the organic-inorganic phase relationship in the two vertebrate skeletal systems (endochondral ossification and calcified cartilage tiles) can provide some hints on the bio-mineralization process discussion. The H_2O molecules and Ca^{2+} and PO_4^{3-} ions transport at level of chondroblasts and osteoblasts cell membrane is the action allowing to reach the critical ions concentration in the extra-cellular space necessary to trigger the Ca_2PO_4 salt deposition on the matrix organic phase elements. The most advanced high resolution analytical and microscopic techniques have shown in the bone collagen type 1 fibrils the earlier, individual crystal deposits characterized by a parallel oriented layout and location in correspondence of inter-fibrils holes and overlapping zones (Fratzl et al., 2004; Landis et al., 1996; Fratzl). No so specific evidence of calcium salts deposits has been so far reported in cartilage type 2 collagen, while other calcium nucleating sites as "matrix vesicles" are the firsts to have been reported in the cartilage organic phase mineralization (Anderson, 1969; Bonucci, 1967). Our study suggests in the examined calcifying tissues a similar mechanism of Ca^{2+} and PO_4^{3-} concentration in the extra-cellular micro-environment carried out either by osteoblasts and chondrocytes by means of ions transport at level of the cell membrane and nucleation on the different organic phase components of the matrix. The derived weight (water loss), crystal sizes and crystallinity defines the mineralogical characters of the inorganic phase, while the mechanical properties of the skeletal segment are determined by the combination of the first with shape, size, structure and layout of the organic phase elements. Another aspect of the large spectrum comparative analysis carried out in this study deserves to be emphasized. Because fluid diffusion in the mineralized tissues have a primary role in the mineral deposition and the growth pattern (Urist, 1961), the vascular and canalicular system of bone tissue assure the fluids circulation and the metabolic exchange among the cells embedded into the calcified bone matrix (Pazzaglia et al., 2012). In the cartilaginous fishes skeleton a comparable system is lacking. However, the mixed texture of collagen calcified fibers network including organic phase components (shown by histochemistry) supported the hypothesis of interstitial fluids diffusion and explained the observation of vital chondrocytes within a calcified tissue lacking of a vascular/canalicular system as that of mammals and teleost fishes. The mineral layout and the associated growth pattern in the Sub-class Chondrichthyes represent a biocalcification model diverging from endochondral ossification which has developed in the course of evolution.

AUTHOR CONTRIBUTIONS

Ugo E. Pazzaglia: Conceptualization; writing – review and editing.
Marcella Reguzzoni: Investigation. **Chiara Milanese:** Formal analysis.

Renata Manconi: Resources. **Luca Lanteri:** Resources. **Tiziana Cubeddu:** Formal analysis. **Guido Zarattini:** Validation. **Piero A. Zecca:** Software. **Mario Raspanti:** Supervision.

ACKNOWLEDGMENTS

The study was carried out using the SEM microscope of the University of Insubria and the light microscopy facilities of the University of Brescia, thanks to a research agreement between the two universities. Mineral analyses were carried out with equipments of Physical Chemistry Division of the University of Pavia. Histochemistry was carried out at DVM University of Sassari. The study was supported by current research funds from DMC at the University of Insubria. The senior author is a retired professor of Orthopedic Surgery from the University of Brescia. The authors acknowledge the contribution to the project development by the Committee of the M. Boni Foundation of Pavia and the valuable support of Dr. Battista Galli, Clinica Veterinaria CMV of Varese for the x-rays documentation.

FUNDING INFORMATION

None of the authors received fundings.


CONFLICT OF INTEREST STATEMENT

The authors declare that they have no competing financial interest or personal relationship that could have influenced the work reported in this paper.

DATA AVAILABILITY STATEMENT

The data that support the findings of this study are available from the corresponding author upon reasonable request.

ORCID

Ugo E. Pazzaglia  <https://orcid.org/0000-0002-3344-2388>
 Marcella Reguzzoni  <https://orcid.org/0000-0003-3738-6632>
 Chiara Milanese  <https://orcid.org/0000-0002-3763-6657>
 Renata Manconi  <https://orcid.org/0000-0002-7619-8493>
 Luca Lanteri  <https://orcid.org/0000-0002-6956-0677>
 Tiziana Cubeddu  <https://orcid.org/0000-0001-7522-8200>
 Guido Zarattini  <https://orcid.org/0000-0002-0161-2434>
 Piero A. Zecca  <https://orcid.org/0000-0001-9646-4958>
 Mario Raspanti  <https://orcid.org/0000-0001-6322-1845>

REFERENCES

- Anderson, H. C. (1969). Vesicles associated with calcification in matrix of epiphyseal cartilage. *The Journal of Cell Biology*, 41, 59–72.
- Applegate, S. P. (1967). A survey of sharks hard parts. In P. W. Gilbert, R. F. Mathewson, & D. P. Rall (Eds.), *Shark, skates and rays* (pp. 37–66). Johns Hopkins Press.
- Biancolillo, A., Tommasetti, M., Bucci, R., Izzo, S., Candillo, F., & Marini, F. (2019). Ancient human bone studied and compared by near infrared spectroscopy, thermogravimetry and chemometrics. *Journal of Near Infrared Spectroscopy*, 27, 6–14.
- Bonucci, E. (1967). Fine structure of early cartilage calcification. *Journal of Ultrastructure Research*, 20, 33–50.
- Bonucci, E. (2007). *Biological calcification* (pp. 491–558). Normal and pathological processes in the early stages. Springer Verlag.
- Bonucci, E. (2013). Chapter 16. In *The mineralization of bone and its analogies with other hard tissues*. Intech Open. <https://doi.org/10.5772/54591>
- Bordat, C. (1988). Les cartilages calcifiés de la petite roussette (*Scyliorhinus canicula* L., Chondrichthyes): Histologie et ultrastructure. *The Canadian Journal of Zoology*, 66, 1432–1445.
- Chamel, J., Schotte, M., Bizzarro, J. J., Zaslansky, P., Fratzi, P., Baum, D., & Dean, M. N. (2020). Co-aligned chondrocytes: Zonal morphological variation and structured arrangement of cell lacunae in tessellated cartilage. *Bone*, 134, 115264.
- Clement, J. G. (1992). Re-examination of the fine structure of endoskeletal mineralization in Chondrichthyes: Implication for growth, ageing and calcium homeostasis. *Australian Journal of Marine & Freshwater Research*, 43, 157.
- Dean, M. N., Mull, C. G., Gorb, S. N., & Summers, A. P. (2009). Ontogeny of the tessellated skeleton: Insight from the skeletal growth of the round stingray *Urolophus halleri*. *Journal of Anatomy*, 215, 227–239.
- Dean, M. N., Youssefpour, H., Earthmann, J. C., Gorb, S. N., & Summers, A. P. (2009). Micro-mechanics and material properties of the tessellated skeleton of cartilaginous fishes. *Integrative and Comparative Biology*, 49, e45.
- Egerbacher, M., Helmreich, M., Mayrhofer, E., & Bock, P. (2006). Mineralisation of hyaline cartilage in the small-spotted dog-fish *Scyliorhinus canicula* L. *Scripta Medica (Brno)*, 79, 199–212.
- Fleish, H., & Neuman, W. F. (1961). Mechanisms of calcification: Role of collagen, polyphosphates, and phosphatase. *The American Journal of Physiology*, 200, 1296–1300.
- Frost, H. M. (1995a). Perspectives: On a “paradigm shift” developing in skeletal science. *Calcified Tissue International*, 56, 1–4.
- Frost, H. M. (1995b). *Introduction to a new skeletal physiology. I: Bone and bones*. Pajaro.
- Frost, H. M. (1996). Perspectives: A proposed general model of the “Mechanostat” (suggestions from a new skeletal-biologic paradigm). *The Anatomical Record*, 244, 139–147.
- Glimcher, M. J. (1989). Mechanism of calcification: Role of collagen fibrils and collagen-phosphoroprotein complexes in vitro and in vivo. *The Anatomical Record*, 224, 139–153.
- Hall, B. K. (2007). *Fins into limbs, evolution*. University of Chicago Press, Chicago, USA.
- Hall, K. C. (2013). ADAM17 controls endochondral ossification by regulating terminal differentiation of chondrocytes. *Molecular and Cellular Biology*, 33, 3077–3090.
- Kemp, N. E., & Westrin, S. K. (1979). Ultrastructure of calcified cartilage in the endoskeletal tesserae of sharks. *Journal of Morphology*, 160, 75–102.
- Landis, W. J., Hodgens, J., Arena, J., Jong, M. S., & McEwen, B. F. (1996). Structural relations between collagen and mineral in bone as determined by high voltage electron microscopy tomography. *Microscopy Research and Technique*, 33, 192–202.
- Maisey, J. G., Denton, J. S. S., Burrow, C., & Pradel, A. (2020). Architectural and ultrastructural features of tessellated calcified cartilage in modern and extinct chondrichthyan fishes. *Journal of Fish Biology*, 98, 919–941. <https://doi.org/10.1111/jfb.14376>
- Nyman, J. S., Reyes, M., & Wang, X. (2005). Effects of ultrastructural changes on the toughness of bone. *Micron*, 36, 566–582.
- Omelon, S., Ariganello, A., Bonucci, E., Grynopas, M., & Nanci, A. (2013). A review of phosphate mineral nucleation in biology and geobiology. *Calcified Tissue International*, 93, 382–396.
- Patonai, Z., Maasz, G., Avar, P., Schmidt, J., Lorand, T., Bajnoczky, I., & Mark, L. (2013). Novel dating method to distinguish between forensic and archeological human skeletal remains by bone mineralization indexes. *International Journal of Legal Medicine*, 127, 529–533.
- Pazzaglia, U. E., Congiu, T., Marchese, M., Zarattini, G., & Dell’Orbo, C. (2012). The canalicular system and the osteoblasts domain in human secondary osteons. *Anatomia Histologia and Embryologia*, 41, 410–418. <https://doi.org/10.1111/5.1439-0264.2012.01150.x>

- Pazzaglia, U. E., Congiu, T., Reguzzoni, M., & Dell'Orbo, C. (2010). The shape modulation of the osteoblast-osteocyte transformation and its correlation with the fibrillar organization in secondary osteons. *Cell and Tissue Research*, 340, 533–540.
- Pazzaglia, U. E., Reguzzoni, M., Casati, L., Sibilia, V., Zarattini, G., & Raspanti, M. (2020a). New morphological evidence of the 'fate' of growth plate hypertrophic chondrocytes in the general context of endochondral ossification. *Journal of Anatomy*, 236, 305–316.
- Pazzaglia, U. E., Reguzzoni, M., Depero, L., Federici, S., Bondioni, M., Zarattini, G., & Raspanti, M. (2020b). The structure of cortical bone as revealed by the application of methods for the calcified matrix study. *Microscopy Research and Technique*, 83, 853–864.
- Pazzaglia, U. E., Reguzzoni, M., Manconi, R., Lanteri, L., Zarattini, G., Zecca, P. A., & Raspanti, M. (2023). Comparative anatomy of the fin system in Batojidea *Raja asterias* and *Torpedo marmorata*: Insights and relationships between musculo-skeletal layout, locomotion and morphology. *Journal of Anatomy*, 1–12. <https://doi.org/10.1111/JOA13881>
- Pazzaglia, U. E., Reguzzoni, M., Manconi, R., Zecca, P. A., Zarattini, G., Campagnolo, M., & Raspanti, M. (2022). The combined cartilage growth-calcification pattern in the wing-fins of Rajidae (Chondrichthyes): A divergent model from endochondral ossification of tetrapods. *Microscopy Research and Technique*, 85, 3642–3652. <https://doi.org/10.1002/jmrt24217>
- Pazzaglia, U. E., Reguzzoni, M., Pagani, F., Sibilia, V., Congiu, T., Salvi, A. G., & Benetti, A. (2018). Study of endochondral ossification in human fetal cartilage anlagen of metacarpals: Comparative morphology of mineral deposition in cartilage and in the periosteal bone matrix. *The Anatomical Record*, 301, 571–580.
- Pazzaglia, U. E., Reguzzoni, M., Saroglia, M., Manconi, R., Zarattini, G., & Raspanti, M. (2022). The complex rostral morphology and the endoskeleton ossification process of two adult samples of *Xiphias gladius* (Xiphiidae). *Journal of Fish Biology*, 101, 42–54.
- Posner, A. S. (1987). Bone mineral and the mineralization process. In W. A. Peck (Ed.), *Bone and mineral researches* (pp. 65–116). Elsevier Science Publisher.
- Schaefer, J. T., & Summers, A. P. (2005). Batoid wing skeletal structure: Novel morphologies, mechanical implications and phylogenetic patterns. *Journal of Morphology*, 264, 298–313.
- Seidel, R., Blumer, M., Pechriggl, E.-J., Lyons, K., Hall, B. K., Fratzl, P., Weaver, J. C., & Dean, M. N. (2017). Calcified cartilage or bone? Collagens in the tessellated endoskeletons of cartilaginous fish (shark and rays). *Journal of Structural Biology*, 200, 54–71.
- Seidel, R., Blumer, M., Zaslansky, P., Knotel, D., Huber, D. R., Weaver, J. C., Fratzl, P., Omelon, S., Bertinetti, L., & Dean, M. N. (2017). Ultrastructural, material and crystallographic description of endphytic masses – A possible damage response in shark and ray tessellated calcified cartilage. *Journal of Structural Biology*, 198, 5–18.
- Seidel, R., Jayasankar, A. K., & Dean, M. N. (2020). The multiscale architecture of tessellated cartilage and its relation to function. *Journal of Fish Biology*, 98(4), 942–955. <https://doi.org/10.1111/jfb.14444>
- Seidel, R., Lyons, K., Blumer, M., Zaslansky, P., Fratzl, P., Weaver, J. C., & Dean, M. N. (2016). Ultrastructural and developmental features of the tessellated endoskeleton of elasmobranchs (sharks and rays). *Journal of Anatomy*, 229, 681–702.
- Takagi, M., Pamley, R. T., Denys, F. R., Yagasaki, H., & Toda, Y. (1984). Ultrastructural cytochemistry of proteoglycans associated with calcification of shark cartilage. *The Anatomical Record*, 208, 149–158.
- Thompson, T. J. U., Gauthier, M., & Islam, M. (2009). The application of a new method of Fourier transform infrared spectroscopy to the analysis of burned bone. *Journal of Archeological Science*, 36, 910–914.
- Urist, M. R. (1961). Calcium and phosphorus in the blood and skeleton of the elasmobranchii. *Endocrinology*, 69, 778–801.
- Zeiger, D. N., Miles, W. C., Eidelman, N., & Lin-Gibson, S. (2011). Cooperative calcium phosphate nucleation within collagen fibrils. *Langmuir*, 27, 8263–8268.

SUPPORTING INFORMATION

Additional supporting information can be found online in the Supporting Information section at the end of this article.

How to cite this article: Pazzaglia, U. E., Reguzzoni, M., Milanese, C., Manconi, R., Lanteri, L., Cubeddu, T., Zarattini, G., Zecca, P. A., & Raspanti, M. (2023). Skeletal calcification patterns of batoid, teleost, and mammalian models: Calcified cartilage versus bone matrix. *Microscopy Research and Technique*, 86(12), 1568–1582. <https://doi.org/10.1002/jemt.24388>